

Original Article

Parametric Optimization in Hydroforming of Nimonic 90 Sheet using Cuckoo Search and Particle Swarm Optimization

J. Fakrudeen Ali Ahamed¹, Pandivelan Chinnaiyan²

^{1,2}School of Mechanical Engineering, Vellore Institute of Technology, Vellore, Tamilnadu, India.

²Corresponding Author : cpandivelan@vit.ac.in

Received: 27 July 2023

Revised: 29 September 2023

Accepted: 09 October 2023

Published: 04 November 2023

Abstract - Hydroforming is used to create parts that are difficult in metal forming. Nimonic 90 sheet operates well at high temperatures and pressures, making it appropriate for aerospace, processing, and industrial applications such as liquefied gas storage, turbine blades, fasteners, etc. This study investigated the optimization of process parameters like pressure, blank holder force and thickness in the hydroforming of Nimonic 90 sheet. In accordance with the standard ASTM E8/E8M, the mechanical properties of Nimonic 90 sheets have been obtained by uniaxial tensile test. The sheet hydroforming process was first simulated using the Finite Element Analysis (FEA) and then validated using experimental data for the maximum pressure required for material failure. Since fully experimental or simulation designs are impractical, the design of experiments using the Box-Behnken Design (BBD) was used to investigate the process parameters. Cuckoo search and particle swarm optimization algorithms were used to predict optimized process parameters to achieve maximum deformation. Validation of the optimized solution is done using FEA and experimentation. Formability is measured by the Forming Limit Diagram (FLD), and maximum deformation is achieved without cracking and wrinkling. The findings revealed that the Cuckoo Search algorithm (CS) gives better results for the optimized process parameters in the formability of the Nimonic 90 sheet. The optimum solution predicted by the CS algorithm is less than 5% deviations from the optimal process parameters, demonstrating the best solution's resilience.

Keywords - Formability, Sheet hydroforming, Nimonic 90, Design of experiments, Particle Swarm Optimization, Cuckoo search algorithm.

1. Introduction

As shown in Figure 1, the hydroforming process has been used to produce components that are difficult to manufacture in metal forming [1]. It manufactures complex geometries with structurally sound components rapidly, effectively, and affordably [1][2][3]. The demand to produce solid, defect-free parts is growing as hydroforming technology is recognized and used extensively in the aircraft and automotive industries [4][5]. The components created by sheet hydroforming can withstand more crash energy since there are no welded joints [6]. Hydroforming can produce all complex geometries of

automobile components such as a front axle, rear axle subframe, dual elbow exhaust manifold, fuel tank, and roofs for luxury class cars [2]. The products that sheet hydroforming produces are very close to the final prescribed geometry and require very little modification because it is a near-net shape manufacturing process [1]. Improved formability in hydroforming is primarily due to strain distributed more evenly, which gives less thinning at the corners [7]. Uniform strain distribution leading to lower thinning at the corners is possible in hydroforming [7].

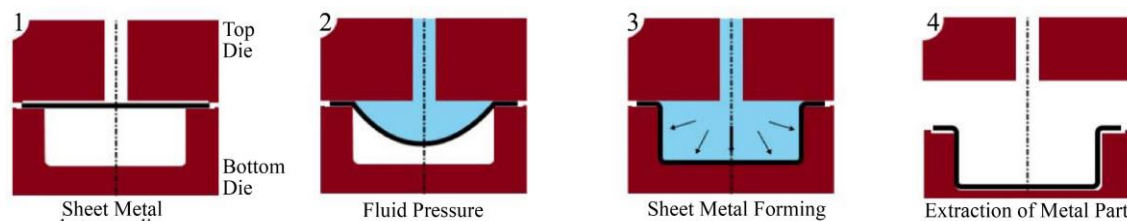


Fig. 1 The Schematic of sheet hydroforming process



Sheet hydroforming process factors include pressure, blank holder force, sheet thickness, and so on. The amount of fluid pressure and the surface area of the blank in contact with the blank holder will determine the Blank Holding Force (BHF). To avoid leaks and uncontrolled material flow, the blank-holder force should be regulated according to the internal pressure [8]. Product quality in sheet metal hydroforming has been considered to be greatly influenced by BHF [9]. The blank area in contact with the blank holder continuously decreases during sheet hydroforming. Hence, adequate BHF is necessary to prevent wrinkling and cracking. Sheet thickness has an impact on formability and forming limits [2].

Understanding the conditions that cause necking (material instability) or fracture in all forming operations that use sheet metal as an input material is critical. Such limits can be represented as a Forming Limit Diagram (FLD) shown in Figure 2, which plots the curve of major and minor strain coordinates [10]. The major strain is always positive and is plotted vertically, while the minor strain is plotted horizontally [11]. A safe operating region is defined by the combination of major and minor strains being below the Forming Limit Curve (FLC), while failure is indicated by the region above the FLC [12]. Primarily for early feasibility studies, formability facilitates the rapid identification of critical areas requiring further examination.

Many researchers have used Finite Element Analysis (FEA) to identify the failure in metal forming[13] [14][15]. FEA and optimization are integrated to achieve optimized process parameters for formability in metal forming [13] [14][15]. In the presence of multiple factors, Design of Experiments (DOE) approaches were used to maximize response variables. DOE is a method for producing desired results using geometric concepts for statistical sampling. The DOE's main objective is to achieve the required response with

the fewest number of trials possible because conducting fewer experiments reduces the cost and time needed to complete the experiments. [13].

Hydroforming has been used on a variety of materials, including steel [16] [17], aluminium alloy [18], Titanium alloy [19] and Nickel alloys [20]. Nickel alloys are long-lasting materials that are capable of withstanding very high temperatures for a long period of time. High-temperature parts of aero-engines and industrial gas turbines use nickel-based superalloys with superior high-temperature tensile strength, greater oxidation resistance, fatigue resistance, corrosion resistance, weldability, and long-term structural stability [21]. The Nimonic 90 alloy belongs to the nickel-based superalloy group. Nimonic 90 is the ideal material to use in exhaust nozzles, gas turbine parts, and aviation parts where the pressure and heat are extremely high [22]. Nimonic 90, despite being strong, is also highly ductile, allowing it to be formed through a variety of different methodologies but at higher pressures than other metals [23].

The primary purpose of hydroforming is to generate low-cost, high-quality products. Optimization techniques enhance the manufacture of the greatest quality products. Metaheuristic algorithms are an example of an optimization technique that can be used to discover the global best solution to a complex function. Because they can handle nonlinear problems and various objectives, these algorithms are frequently utilized in the optimization of process parameters in manufacturing. In many scientific applications, many researchers used a variety of population-based optimization techniques, such as the genetic algorithm, differential evolution, particle swarm optimization, and cuckoo search algorithms have been preferred because they are more successful than gradient techniques at locating the best response [24].

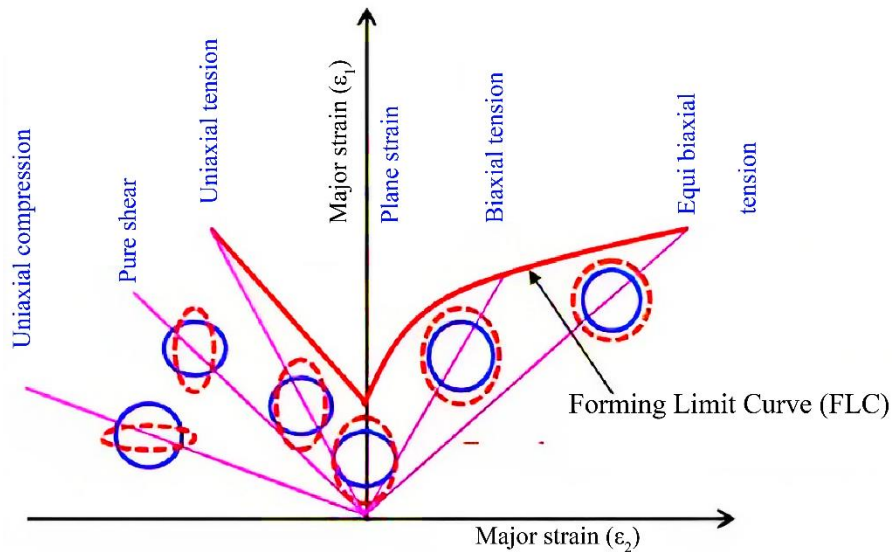


Fig. 2 The Illustrative of FLD

PSO is regarded as a resilient stochastic optimization algorithm since it is less sensitive to the factors that are special to the algorithm than other evolutionary algorithms [25]. The PSO method has been applied to process optimization. A few PSO-based approaches have been developed to optimize the single-response optimization process [26].

The CS approach runs randomly using Lévy flights rather than basic isotropic random search, which improves the algorithm's search performance and provides some advantages in tackling function optimization problems. Fewer parameters, easy operation, uncomplicated implementation, strong random search path optimization and optimization skills, and the capacity to converge to the global optimal are the key benefits of the CS algorithm [27].

The following details were included in the summary of the literature-reviewed papers:

- Sheet hydroforming process
- FLD and its advantages
- Nimonic alloy and its applications
- The problem of optimization, which involves manufacturing process parameters and responses,
- Need of Optimization

Existing studies lack the optimization of process parameters in the hydroforming of Nimonic alloys. To the best of the authors' knowledge, this is the first attempt to optimize the hydroforming process of the nimonic 90 sheets using PSO

and CS algorithms. The scope of this study is to propose an optimized model and a better optimization algorithm for optimizing process parameters in hydroforming.

In this study, the following objectives will help to achieve the goal:

- Derivation of FEA model for sheet hydroforming;
- DoE and formation of regression equation;
- Optimal response using optimization approaches;
- Determination of optimum process parameters for hydroforming of Nimonic 90 sheet;
- Confirmation of optimum process parameters with FEA and experimentation;
- Evaluation of forming limit diagram;
- Discussion of the FEA model's accuracy.

2. Material and Methodology

In this section, details of material composition and its properties, Modeling, FEA simulation, experimentation, DOE, and optimization methods used are discussed.

2.1. Material & its Properties

The material used in this study was nimonic 90 sheet. Its composition and mechanical properties were taken from the author's previous study [2] and illustrated in Tables 1 and 2, respectively.

Uniaxial tensile tests were performed in accordance with ASTM E8/E8M standards, as indicated in Figure 3.

Table 1. Nimonic 90 sheet composition [2]

S	P	C	Cu	Si	Mn	Fe	Al	Ti	Co	Cr	Ni
0.007	0.008	0.082	0.085	0.34	0.67	0.98	1.38	2.37	16.73	18.65	Balance

Table 2. Nimonic 90 sheet - Mechanical properties [2]

Material Properties	Value
Modulus of Elasticity	105.95 x 10 ³ MPa
Yield Stress (0.2%)	587 x 10 ⁶ Pa
Ultimate Tensile Stress	1271 x 10 ⁶ Pa
Poisson's Ratio	0.28
Strain Hardening Exponent at n value	0.3039
Strength Coefficient at n value	1555.3697

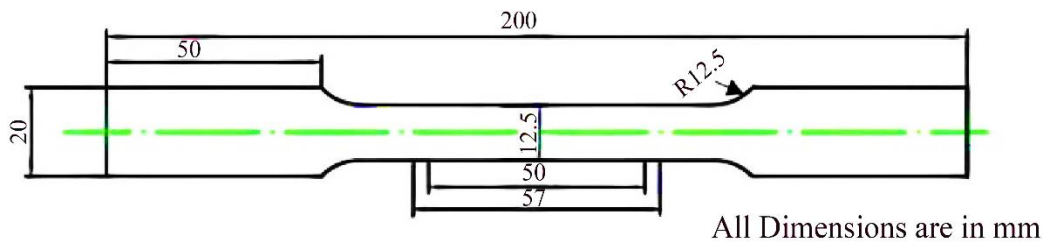


Fig. 3 Illustrative of tensile test specimen (ASTM E8/E8M)

Table 3. Sheet and die dimension

Component	Dimension (mm)
Nimonic 90 Sheet	65 x 65
Nimonic 90 Sheet Thickness	0.8, 1 & 1.2
Top Die	100 x 100
Bottom Die	100 x 100
Die Cavity	38 x 38 x 20
Die Corner Radius	04 to 05

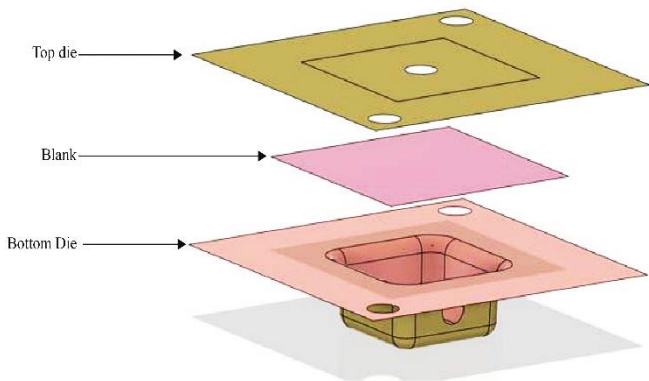


Fig. 4 CAD Model of die and sheet

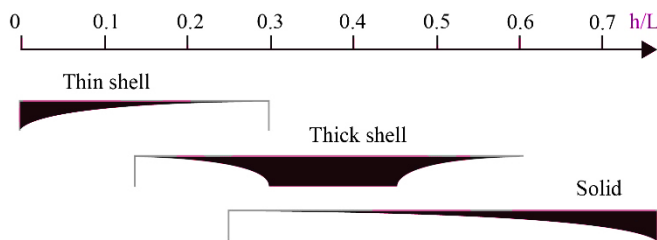


Fig. 5 Schematic of h/L chart [15]

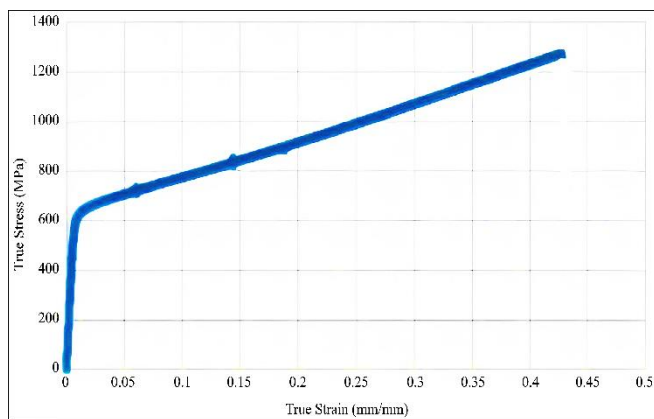


Fig. 6 True Stress—Strain curve of nimonic 90 Sheet

2.2. CAD Modeling and Simulation

In this study, components are modeled as shell elements for Finite Element Analysis (FEA) simulations using the Autodesk Fusion 360 software, as illustrated in Figure 4.

Because shell elements enable the modeling of narrow features with fewer mesh components, FEA utilizes them to attain better results and lower the computational time [28]. The thin shell approximation is used in this model since the thickness-to-length ratio (h/L Chart) is within 0.3, according to the approximation model presented in Figure 5. [29]. In FEA simulation, the thickness of all surface components is assigned. Table 3 illustrates the dimensions of all components used in CAD modeling. The radius of the die corner should be greater than four times the material thickness [30].

2.2.1 Finite Element Simulation

Two regions, elastic and plastic regions, were considered when defining the properties of the Nimonic 90 sheet. The elastic properties were assigned as shown in Table 2, and the true stress and strain of the material's plastic region were shown in Figure 6. Ansys Mechanical was used for meshing. Quadrilateral elements were chosen for meshing because they produced far smoother surfaces than triangular elements, which frequently produced apparent anomalies on the surface [31]. All the free elements were set to quad type, with a 2 mm element size. Using the face sizing option, several key areas, such as the blank surface, fillets, and corner surfaces, are defined with lower element sizes of 1 mm. After creating the mesh, it is exported to LS Dyna in STL format. LS-Dyna explicit solver is used for its extensive features of FLD, thinning percentages, and drawing beads. BHF is loaded on the top die, and Pressure is applied on the top of the sheet. A drawbead depth of 1mm is chosen for the analysis. Mesh refinement for convergence study was carried out in this work. Simulations for various mesh refining phases were performed.

2.3. Experimental Model

Experiment work was carried out utilizing a 100-ton hydraulic press and a 1000-bar pressure pump to validate the results of numerical simulations and decide on the optimum process parameters. Table 3 shows the dimensions of the die and sheet that were used.

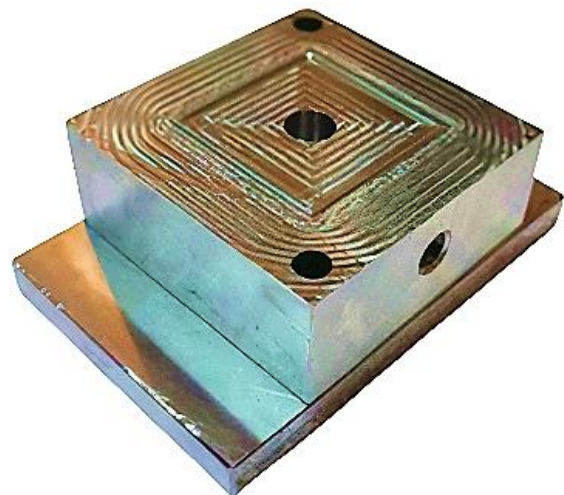


Fig. 7 Top die and plate

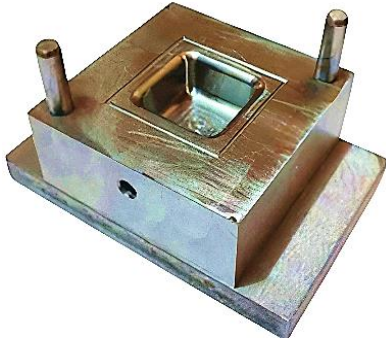


Fig. 8 Bottom die and plate

The dies depicted in Figures 7 and 8 were manufactured out of P20 tool steel, which has a high degree of deformation resistance [32]. The top and bottom plates were connected to their corresponding dies by M8 bolts, enabling the hydraulic press to clamp the die. Using a laser cutting machine, the specimen, Nimonic 90, depicted in Figure 9, was cut according to the dimensions.

The validation experiment was carried out for maximum pressure. As the finite element simulation was validated using the experimental model and found to be within acceptable limits, the same FEA simulation approach was also used to design experiments.

2.4. Design of Experiments

The experiments were developed using the Box-Behnken Design (BBD) of Response Surface Methodology (RSM) by employing lower and higher levels of variable factors such as Pressure (Pr), Blank Holder Force (BHF), and sheet Thickness (T), as shown in Table 4, yielding 15 experiments to run using Minitab software. Table 5 illustrates the conditions under which the simulations were performed.

Table 4. Process parameters and its levels

Process Parameters	Lower Level	Higher Level
Pressure (MPa)	30	50
BHF(kN)	180	220
Thickness (mm)	0.8	1.2

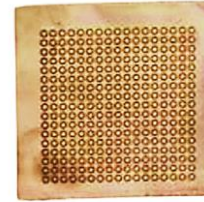


Fig. 9 Nimonic 90 sheet specimen

2.5. Proposed Methods

In this section, two nature-based algorithms, Particle Swarm Optimization (PSO) and Cuckoo Search Algorithm (CS), are used to find optimal process parameters in the formability of nimonic 90 sheets in the hydroforming process.

2.5.1. PSO Algorithm

At present, the PSO algorithm is used to solve real-world problems in all fields. PSO determines the fitness function's single value. The PSO method can be used to solve large-scale optimization problems. [33]. PSO finds the optimal solution through particle interaction but converges to the global optimum rather slowly in a high-dimensional search space [34].

Table 5. Design of experiments- BBD

Run Order	Standard Order	Block	Pt Type	Thickness (mm)	Pressure (MPa)	BHF (kN)
1	14	1	0	1	40	180
2	4	1	2	1	50	220
3	12	1	2	1.2	40	220
4	1	1	2	1	30	140
5	3	1	2	1	30	220
6	15	1	0	1	40	180
7	6	1	2	0.8	50	180
8	8	1	2	1.2	50	180
9	9	1	2	0.8	40	140
10	10	1	2	0.8	40	220
11	11	1	2	1.2	40	140
12	13	1	0	1	40	180
13	7	1	2	1.2	30	180
14	2	1	2	1	50	140
15	5	1	2	0.8	30	180

The selection of the global best is an important step in this algorithm. Because of this, both the diversity and convergence criteria of non-dominated solutions are affected. The search is conducted in all directions; the global best guide is chosen based on crowding distance calculation. Typically, the solution with the greatest crowding distance is regarded as the best global guide. As a result, the search has been broadened to encompass all dimensions. When the external archive for non-dominated solutions becomes full, the solutions are replaced using the crowding distance calculation. The solution in a densely populated region is replaced by the

new solution to maintain a good spread of solutions. As a result, the algorithm generates a diverse set of solutions [33]. PSO's performance is highly reliant on the settings (maximum and minimum value of parameters, i.e. pressure, blank holder force and thickness) that are chosen. The algorithm used in this study is based on the PSO flowchart as illustrated in Figure 10.

In this study, to achieve the best performance from the PSO algorithm, The PSO parameters shown in Table 6 were determined by the trial and error approach.

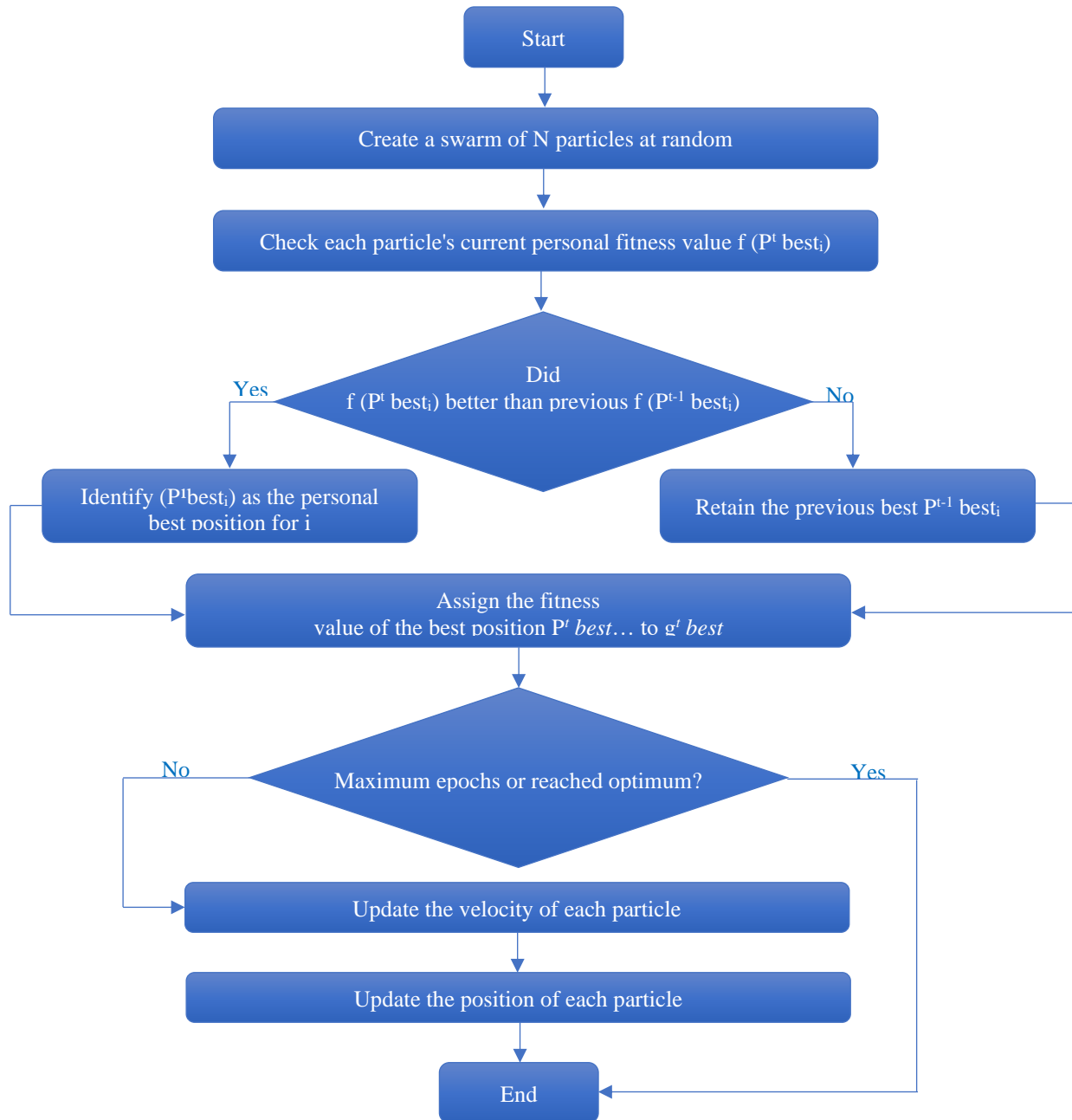


Fig. 10 PSO flowchart

Table 6. PSO parameters and its values

PSO Parameters	Value
Size of the swarm (no. of birds), n	50
Maximum number of bird steps	100
Dimension of the problem	3
C1	0.12
C2	1.2
PSO Momentum or inertia w	0.9

2.5.2. Cuckoo Search Algorithm

Another population-based stochastic algorithm that draws inspiration from cuckoos' breeding procedures is the Cuckoo Search Algorithm (CS) [35]. Because of their unique lifestyle and aggressive reproductive tactics, various species of the bird family known as cuckoo are the inspiration for the CS [24]. Cuckoos employ a number of techniques to reduce the likelihood of being abandoned by their hosts. Yang and Deb first introduced the cuckoo search in 2009 [36], and it was subsequently implemented in engineering optimization.

The pseudo-code for the CS algorithm [37] is as follows
begin

Objective function $f(x)$, $x = (x_1, \dots, x_d)^T$
Generate initial population of n host nests x_i ($i = 1, 2, \dots, n$)
while ($t < \text{MaxGeneration}$) *or* (*stop criterion*)
Get a cuckoo at random from Levy flights
evaluate its fitness/ quality F_i
Choose a nest among n (say, j) randomly
if ($F_i > F_j$),
the new solution is replaced by j;
end
New nests are built by abandoning a fraction (pa) of worse nests;
The best solutions (or nests with quality solutions) should be kept;
Rank the solutions and identify the current best
end while
Postprocess results and visualization
End

The CS parameters shown in Table 7 were determined by the trial and error approach.

Table 7. CS parameters and its values

CS Parameters	Value
Number of initial populations	50
Minimum number of eggs for each cuckoo	2
Maximum number of eggs for each cuckoo	4
Maximum iterations of the Cuckoo Algorithm	100
Maximum number of cuckoos that can live at the same time	200
Control parameter of egg-laying	50

3. Result and Discussion

The maximum pressure obtained during hydroforming in FEA simulation and experiment is shown in Table 8. As the error percentage between simulation and experiment is less than 10%, it suggests that the proposed simulation model can provide accurate predictions [38] [39]. The finite element simulation process was then performed under various conditions based on the design of experiments (Table 5), and the response variable, i.e., deformation (De), resulted, as shown in Table 9.

In the author's previous study [2], an RSM optimizer is used to predict the optimal process parameter for hydroforming of Nimonic 90 sheets. Fluid pressure (Pr), blank holder force (BHF) and thickness (T) of the specimen have the greatest effect on the hydroforming of the nimonic 90 sheets. In the optimization of parameters for hydroforming, the purpose is to maximize the deformation (objective function) without failure. The deformation (De) is defined as follows [2].

$$De = 8.52 + 0.3483 \times Pr - 0.00044 \times BHF - 14.59 \times T + 0.000262 \times Pr \times Pr - 0.000001 \times BHF \times BHF + 7.344 \times T \times T - 0.000000 \times Pr \times BHF - 0.1925 \times Pr \times T + 0.00031 \times BHF \times T \quad (1)$$

The optimization is carried out in the proposed methods using equation (1) and the lower and upper bound values of process parameters shown in Table 4 to achieve the maximum deformation.

Table 8. Maximum pressure obtained by FEA simulation & experiment

	Maximum Pressure (MPa)	Percentage Error (%)
FEA Simulation	53.46	5.53
Experimentation	50.5	

Table 9. Deformation results obtained from FEA simulation

Run Order	Inputs			Output
	Pr (MPa)	BHF (kN)	T (mm)	De (mm)
1	40	180	1	7.88
2	50	220	1	9.62
3	40	220	1.2	6.65
4	30	140	1	6.19
5	30	220	1	6.16
6	40	180	1	7.88
7	50	180	0.8	11.9
8	50	180	1.2	8.11
9	40	140	0.8	9.7
10	40	220	0.8	9.66
11	40	140	1.2	6.68
12	40	180	1	7.88
13	30	180	1.2	5.27
14	50	140	1	9.65
15	30	180	0.8	7.52

Table 10. Optimal results for maximum deformation without failure

Methods	Process Parameters			Output Response-Deformation (mm)
	Pressure (MPa)	BHF (kN)	Thickness (mm)	
CS	47.81	165.45	0.8	11.378
PSO	47.64	165.54	0.83	10.988
RSM optimizer [2]	42.32	144.04	0.8	10.199

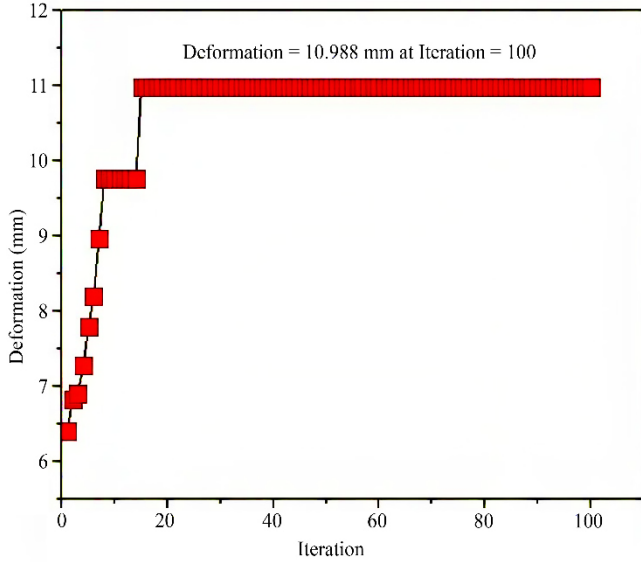


Fig. 11 Convergence graph of PSO algorithm

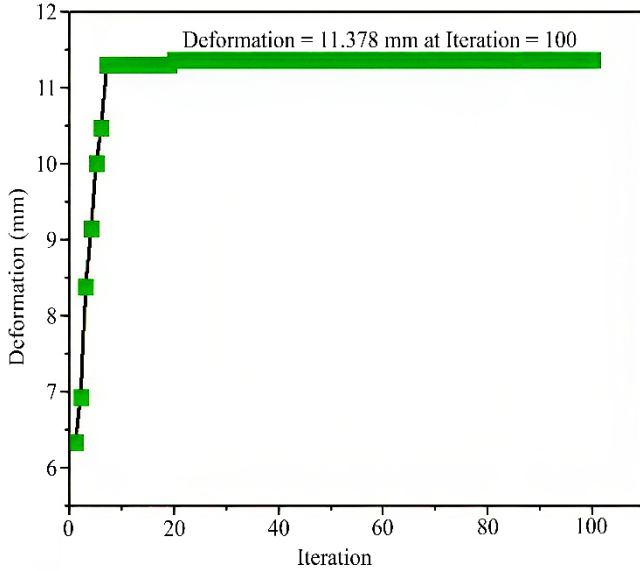


Fig. 12 Convergence graph of CS algorithm

Table 10 compares the results generated by the CS algorithm with the ones obtained by PSO, and both algorithms give better results than the RSM optimizer. The convergence graph of the PSO and CS algorithm for the maximum deformation obtained is illustrated in Figures 11 and 12, respectively.

A confirmatory FEA simulation and experiment were conducted in this study to verify the accuracy of the optimized result obtained by the CS algorithm. Figure 13 depicts the confirmatory FEA simulation result. The experimental validation result shown in Figure 14 depicts the deformed nimonic sheet for the optimum process parameters obtained by the CS approach.

Table 11 illustrates the predicted (CS), FEA simulation and experimental results for achieving maximum deformation of the nimonic 90 sheet without failure. Since the error percentage between predicted (CS), FEA simulation and experimental results was less than 5%, the proposed approach (CS) can provide accurate predictions.

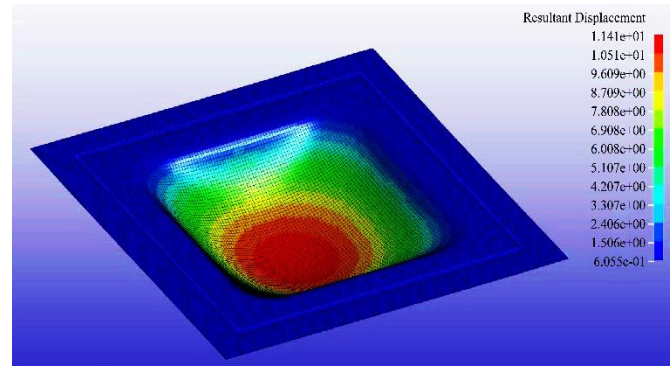


Fig. 13 FEA Simulation result of maximum deformation for optimized parameters

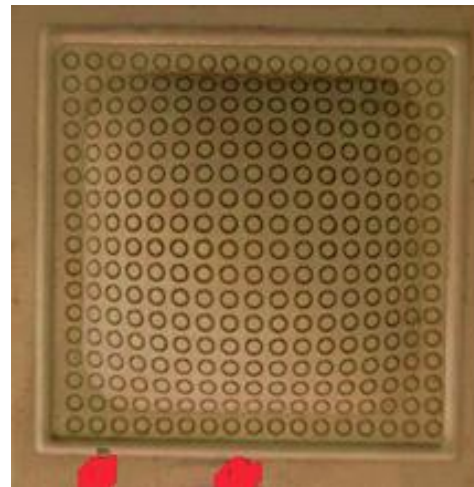


Fig. 14 Experimental validation for optimized parameters

Table 11. Confirmatory simulation and experimental results with CS algorithm result

Process Parameter			CS-Predicted deformation (mm)	Deformation (mm)		% of error	
Pressure (MPa)	BHF (kN)	T (mm)		Simulation	Experimental	Simulation	Experimental
47.81	165.45	0.8	11.378	11.41	11.29	0.28	0.77

The major and minor strains of Nimonic 90 during hydroforming for the optimized process parameters are depicted in the forming limit diagram created using LSdyna, as illustrated in Figure 15. Strain combinations above the FLC result in fracture, whereas those that fall below the wrinkling limit line result in wrinkles.

For a constant minor strain, a wider gap between the FLC and wrinkling limit lines indicates a greater possibility of forming [40]. Since the space between the FLC and the wrinkling limit line was greater in the FLD, as illustrated in Figure 15, the Nimonic 90 sheet was better suited for forming.

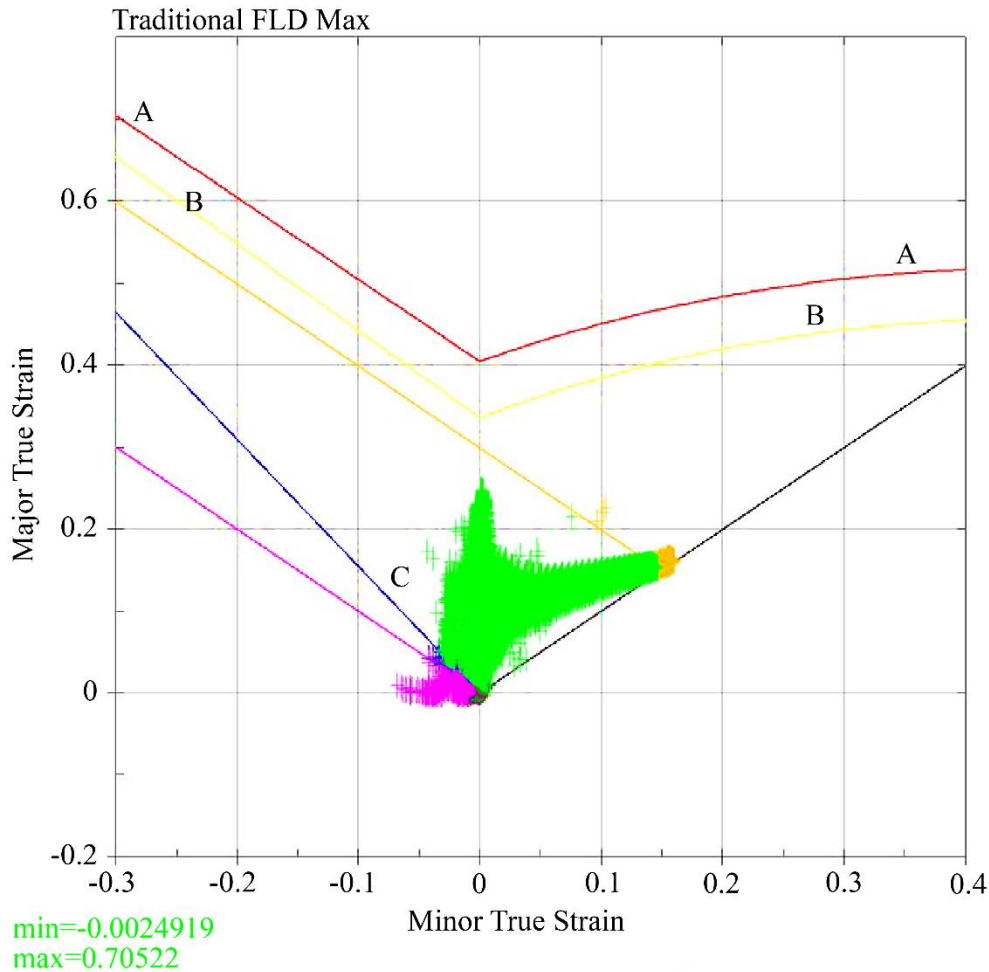


Fig. 15 Forming Limit Diagram for optimized parameters in Nimonic 90 - Safe Severe thinning. (A) Forming limit curve (FLC), (B) Risk of Failure, (C) Wrinkling limit line

4. Conclusion

This study used two optimization approaches, PSO and CS algorithms, to investigate the optimum process parameters, pressure, blank holder force, and thickness in the hydroforming of Nimonic 90 sheet and formability study based on the FLD. The key findings of this study can be described concisely as follows.

- To determine the formability, a proper FEA model was developed and to obtain optimum process parameters,

PSO and CS algorithms were used; the results show that the CS algorithm gives better results than the PSO approach;

- Based on the optimization and verified simulation and experiments, the important parameters for preventing wrinkling during the forming state and achieving maximum deformation were BHF of 165.45 kN, pressure of 47.81 MPa and sheet thickness of 0.8 mm,

- The formability of the Nimonic 90 sheet tested was good for all strain conditions.
- In comparison to the tension-compression condition, the formability was greater under conditions of plane strain and biaxial tension;
- During sheet hydroforming, the fluid pressure caused the sheet to stretch in the flange area, causing strains above the wrinkling limit curve in the Forming Limit Diagram (FLD), which is a favourable condition for forming;
- Since the FLD obtained by simulation indicated no failure zone, these optimum process parameter values were acceptable.

Future studies will focus on applying the same methodology for checking the formability of other superalloys, and the same can be implemented for complex geometry parts.

Author Contributions

F.A.A was responsible for design, FEA and optimization; P.C. was responsible for the experimentation study and behavior study. All authors have read and agreed to the published version of the manuscript.

Data Availability Statement

The data presented in this study are available on request from the corresponding author.

References

- [1] Shijian Yuan, "Fundamentals and Processes of Fluid Pressure Forming Technology for Complex Thin-Walled Components," *Engineering*, vol. 7, no. 3, pp. 358–366, 2021. [[CrossRef](#)] [[Google Scholar](#)] [[Publisher Link](#)]
- [2] S. Sandhiya, and U. Palani, "A Novel Hybrid PSBCO Algorithm for Feature Selection," *International Journal of Computer and Organization Trends*, vol. 10, no. 3, pp. 21-26, 2020. [[CrossRef](#)] [[Google Scholar](#)] [[Publisher Link](#)]
- [3] Myoung-Gyu Lee, Yannis P. Korkolis, and Ji Hoon Kim, "Recent Developments in Hydroforming Technology," *Proceedings of the Institution of Mechanical Engineers, Part B: Journal of Engineering Manufacture*, vol. 229, no. 4, pp. 572–596, 2015. [[CrossRef](#)] [[Google Scholar](#)] [[Publisher Link](#)]
- [4] P. Venkateshwar Reddy, B. Veerabhadra Reddy, and P. Janaki Ramulu, "An Investigation on Tube Hydroforming Process Considering the Effect of Frictional Coefficient and Corner Radius," *Advances in Materials and Processing Technologies*, vol. 6, no. 1, pp. 84–103, 2020. [[CrossRef](#)] [[Google Scholar](#)] [[Publisher Link](#)]
- [5] Bo Liu et al., "Development and Application of Magnesium Alloy Parts for Automotive Oems: A Review," *Journal of Magnesium and Alloys*, vol. 11, no. 1, pp. 15–47, 2023. [[CrossRef](#)] [[Google Scholar](#)] [[Publisher Link](#)]
- [6] E. Pavithra, and V.S. Senthil Kumar, "Microstructural Evolution of Hydroformed Inconel 625 Bellows," *Journal of Alloys and Compounds*, vol. 669, pp. 199–204, 2016. [[CrossRef](#)] [[Google Scholar](#)] [[Publisher Link](#)]
- [7] Huiting Wang, and Xiaohui Shen, "A Novel Hydrodynamic Deep Drawing Utilizing a Combined Floating and Static Die Cavity," *The International Journal of Advanced Manufacturing Technology*, vol. 114, no. 3–4, pp. 829–839, 2021. [[CrossRef](#)] [[Google Scholar](#)] [[Publisher Link](#)]
- [8] Shijian Yuan, and Xiaobo Fan, "Developments and Perspectives on the Precision Forming Processes for Ultra-Large Size Integrated Components," *International Journal of Extreme Manufacturing*, vol. 1, no. 2, 2019. [[CrossRef](#)] [[Google Scholar](#)] [[Publisher Link](#)]
- [9] Thu Thi Nguyen, and Trung Dac Nguyen, "A Study on the Impact of Blank Holder Pressure on Forming Pressure and Product Quality in Hydrostatic Forming," *International Journal of Precision Engineering and Manufacturing*, vol. 24, no. 2, pp. 187–198, 2023. [[CrossRef](#)] [[Google Scholar](#)] [[Publisher Link](#)]
- [10] Zahra Ramezani Anbaran et al., "Generalized Phenomenological Model to Analyze the Forming Limit Curve of Al 1050," *The Journal of Strain Analysis for Engineering Design*, vol. 58, no. 7, pp. 582–589, 2023. [[CrossRef](#)] [[Google Scholar](#)] [[Publisher Link](#)]
- [11] I. Pätzold et al., "Reducing the Shear Affected Zone to Improve the Edge Formability Using a Two-Stage Shear Cutting Simulation," *Journal of Materials Processing Technology*, vol. 313, 2023. [[CrossRef](#)] [[Google Scholar](#)] [[Publisher Link](#)]
- [12] Paulina Lisiecka-Graca et al., "Application of the DIC System to Build a Forming Limit Diagram(FLD) of Multilayer Materials," *Key Engineering Materials*, vol. 926, pp. 963–969, 2022. [[CrossRef](#)] [[Google Scholar](#)] [[Publisher Link](#)]
- [13] M.R. Jamli, and N.M. Farid, "The Sustainability of Neural Network Applications within Finite Element Analysis in Sheet Metal Forming: A Review," *Measurement*, vol. 138, pp. 446–460, 2019. [[CrossRef](#)] [[Google Scholar](#)] [[Publisher Link](#)]
- [14] Mohd. Ahmed, "Adaptive Finite Element Simulation of Sheet Forming Process Parameters," *Journal of King Saud University - Engineering Sciences*, vol. 30, no. 3, pp. 259–265, 2018. [[CrossRef](#)] [[Google Scholar](#)] [[Publisher Link](#)]
- [15] Xiangwei Kong et al., "Experimental and Finite Element Optimization Analysis on Hydroforming Process of Rupture Disc," *Procedia Manufacturing*, vol. 15, pp. 892–898, 2018. [[CrossRef](#)] [[Google Scholar](#)] [[Publisher Link](#)]
- [16] Morteza Hosseinzadeh, "The Effect of Polyurethane Hardness on the New Die-Set of Sheet Hydroforming Process Parameters," *Applied Mechanics and Materials*, vol. 152–154, pp. 1623–1627, 2012. [[CrossRef](#)] [[Google Scholar](#)] [[Publisher Link](#)]
- [17] Radu Vasile, Sever-Gabriel Racz, and Octavian Bologna, "Experimental and Numerical Investigations of the Steel Sheets Formability With Hydroforming," *The 4th International Conference on Computing and Solutions in Manufacturing Engineering 2016 – CoSME'16*, vol. 94, 2017. [[CrossRef](#)] [[Google Scholar](#)] [[Publisher Link](#)]

- [18] Cristina Churiaque et al., “Springback Estimation in the Hydroforming Process of UNS A92024-T3 Aluminum Alloy by FEM Simulations,” *Metals*, vol. 8, no. 6, pp. 1-17, 2018. [[CrossRef](#)] [[Google Scholar](#)] [[Publisher Link](#)]
- [19] Gaoshen Cai et al., “A Novel Approach to Predict Wrinkling of Aluminum Alloy During Warm/Hot Sheet Hydroforming Based on an Improved Yoshida Buckling Test,” *Materials*, vol. 13, no. 5, pp. 1-19, 2020. [[CrossRef](#)] [[Google Scholar](#)] [[Publisher Link](#)]
- [20] Colin Bell et al., “Enabling Sheet Hydroforming to Produce Smaller Radii on Aerospace Nickel Alloys,” *International Journal of Material Forming*, vol. 12, no. 5, pp. 761–776, 2019. [[CrossRef](#)] [[Google Scholar](#)] [[Publisher Link](#)]
- [21] D. Clark et al., “Shaped Metal Deposition of a Nickel Alloy for Aero Engine Applications,” *Journal of Materials Processing Technology*, vol. 203, no. 1–3, pp. 439–448, 2008. [[CrossRef](#)] [[Google Scholar](#)] [[Publisher Link](#)]
- [22] Navneet Khanna et al., “Optimization of Power Consumption Associated with Surface Roughness in Ultrasonic Assisted Turning of Nimonic-90 Using Hybrid Particle Swarm-Simplex Method,” *Materials*, vol. 12, no. 20, pp. 1-20, 2019. [[CrossRef](#)] [[Google Scholar](#)] [[Publisher Link](#)]
- [23] Arun Kumar Pandey, and Girish Dutt Gautam, “Grey Relational Analysis-Based Genetic Algorithm Optimization of Electrical Discharge Drilling Of Nimonic-90 Superalloy,” *Journal of the Brazilian Society of Mechanical Sciences and Engineering*, vol. 40, no. 3, 2018. [[CrossRef](#)] [[Google Scholar](#)] [[Publisher Link](#)]
- [24] Ali R. Yildiz, “Cuckoo Search Algorithm for the Selection of Optimal Machining Parameters in Milling Operations,” *The International Journal of Advanced Manufacturing Technology*, vol. 64, no. 1–4, pp. 55–61, 2013. [[CrossRef](#)] [[Google Scholar](#)] [[Publisher Link](#)]
- [25] Tatjana V. Sibalija, “Particle Swarm Optimisation in Designing Parameters of Manufacturing Processes: A Review (2008–2018),” *Applied Soft Computing*, vol. 84, 2019. [[CrossRef](#)] [[Google Scholar](#)] [[Publisher Link](#)]
- [26] Liangshan Shao et al., “Particle Swarm Optimization Algorithm Based on Semantic Relations and Its Engineering Applications,” *Systems Engineering Procedia*, vol. 5, pp. 222–227, 2012. [[CrossRef](#)] [[Google Scholar](#)] [[Publisher Link](#)]
- [27] Dili Shen et al., “A Cuckoo Search Algorithm Using Improved Beta Distributing and its Application in the Process of EDM,” *Crystals*, vol. 11, no. 8, pp. 1-15, 2021. [[CrossRef](#)] [[Google Scholar](#)] [[Publisher Link](#)]
- [28] Radu Vasile, Sever-Gabriel Racz, and Octavian Bologa, “Numerical and Experimental Analysis of the Formability of 1.4301 Austenitic Stainless Steel Sheets Using Hydroforming,” *Proceedings in Manufacturing Systems*, vol. 11, no. 2, pp. 89–94, 2016. [[Google Scholar](#)] [[Publisher Link](#)]
- [29] T. Mazúch et al., “Natural Modes and Frequencies of a Thin Clamped–Free Steel Cylindrical Storage Tank Partially Filled With Water: Fem and Measurement,” *Journal of Sound and Vibration*, vol. 193, no. 3, pp. 669–690, 1996. [[CrossRef](#)] [[Google Scholar](#)] [[Publisher Link](#)]
- [30] Schuler GmbH, “Sheet Metal Forming and Blanking,” *Metal Forming Handbook*, pp. 123–404, 1998. [[CrossRef](#)] [[Publisher Link](#)]
- [31] J. Baumgartner, and T. Bruder, “An Efficient Meshing Approach for the Calculation of Notch Stresses,” *Welding in the World*, vol. 57, no. 1, pp. 137–145, 2013. [[CrossRef](#)] [[Google Scholar](#)] [[Publisher Link](#)]
- [32] Guanghua Yan et al., “Wear and Corrosion Behavior of P20 Steel Surface Modified by Gas Nitriding with Laser Surface Engineering,” *Applied Surface Science*, vol. 530, 2020. [[CrossRef](#)] [[Google Scholar](#)] [[Publisher Link](#)]
- [33] S. Mahalakshmi, A. Arokiasamy, and J. Fakrudeen Ali Ahamed, “Productivity Improvement of an Eco Friendly Warehouse using Multi Objective Optimal Robot Trajectory Planning,” *International Journal of Productivity and Quality Management*, vol. 27, no. 3, pp. 305-328, 2019. [[CrossRef](#)] [[Google Scholar](#)] [[Publisher Link](#)]
- [34] Ahmed G. Gad, “Particle Swarm Optimization Algorithm and its Applications: A Systematic Review,” *Archives of Computational Methods in Engineering*, vol. 29, no. 5, pp. 2531–2561, 2022. [[CrossRef](#)] [[Google Scholar](#)] [[Publisher Link](#)]
- [35] Rui Chi et al., “A Hybridization of Cuckoo Search and Differential Evolution for the Logistics Distribution Center Location Problem,” *Mathematical Problems in Engineering*, 2019. [[CrossRef](#)] [[Google Scholar](#)] [[Publisher Link](#)]
- [36] Xin-She Yang, and Suash Deb, “Cuckoo Search via Lévy Flights,” *World Congress on Nature & Biologically Inspired Computing*, pp. 210–214, 2009. [[CrossRef](#)] [[Google Scholar](#)] [[Publisher Link](#)]
- [37] Sanjay Agrawal et al., “Tsallis Entropy Based Optimal Multilevel Thresholding Using Cuckoo Search Algorithm,” *Swarm and Evolutionary Computation*, vol. 11, pp. 16–30, 2013. [[CrossRef](#)] [[Google Scholar](#)] [[Publisher Link](#)]
- [38] Masoud Rahiminezhad Galankashi et al., “Performance Evaluation of a Petrol Station Queuing System: A Simulation-Based Design of Experiments Study,” *Advances in Engineering Software*, vol. 92, pp. 15–26, 2016. [[CrossRef](#)] [[Google Scholar](#)] [[Publisher Link](#)]
- [39] Dungang Liu et al., “A New Goodness-of-Fit Measure for Probit Models: Surrogate R^2 ,” *British Journal of Mathematical and Statistical Psychology*, vol. 76, no. 1, pp. 192–210, 2023. [[CrossRef](#)] [[Google Scholar](#)] [[Publisher Link](#)]
- [40] Surajit Kumar Paul, “Controlling Factors of Forming Limit Curve: A Review,” *Advances in Industrial and Manufacturing Engineering*, vol. 2, 2021. [[CrossRef](#)] [[Google Scholar](#)] [[Publisher Link](#)]